

Article

Equilibrium and Kinetics of CO₂ Adsorption by Coconut Shell Activated Carbon Impregnated with Sodium Hydroxide

Chaiyot Tangsathitkulchai ^{1,*}, Suravit Naksusuk ¹, Atichat Wongkoblap ¹, Poomiwat Phadungbut ² and Prapassorn Borisut ¹

¹ School of Chemical Engineering, Institute of Engineering, Suranaree University of Technology, Muang District, Nakhon Ratchasima 30000, Thailand; suravit@sut.ac.th (S.N.); atichat@sut.ac.th (A.W.); prapatsorn.borisut@gmail.com (P.B.)

² Department of Chemical Engineering, Faculty of Engineering, Mahidol University, Nakhon Pathom 73170, Thailand; poomiwat.pha@mahidol.ac.th

* Correspondence: chaiyot@sut.ac.th; Fax: +66-44-22-4420

Abstract: The equilibrium and kinetics of CO₂ adsorption at 273 K by coconut-shell activated carbon impregnated with sodium hydroxide (NaOH) was investigated. Based on nitrogen adsorption isotherms, porous properties of the tested activated carbons decreased with the increase of NaOH loading, with the decrease resulting primarily from the reduction of pore space available for nitrogen adsorption. Equilibrium isotherms of CO₂ adsorption by activated carbons impregnated with NaOH at 273 K and the pressure up to 100 kPa displayed an initial part of Type I isotherm with most adsorption taking place in micropores in the range of 0.7–0.9 nm by pore-filling mechanisms. The amount of CO₂ adsorbed increased with the increase of NaOH loading and passed through a maximum at the optimum NaOH loading of 180 mg/g. The CO₂ isotherm data were best fitted with the three-parameter Sips equation, followed by Freundlich and Langmuir equations. The pore diffusion model, characterized by the effective pore diffusivity (D_e), could well describe the adsorption kinetics of CO₂ in activated carbons impregnated with NaOH. The variation of D_e with the amount of CO₂ adsorbed showed three consecutive regions, consisting of a rapid decrease of D_e for CO₂ loading less than 40 mg/g, a relatively constant value of D_e for the CO₂ loading of 40–80 mg/g and a slow decrease of D_e for the CO₂ loading of 80–200 mg/g. The maximum D_e occurred at the optimum NaOH loading of 180 mg/g, in line with the equilibrium adsorption results. The values of D_e varied from 1.1×10^{-9} to 5.5×10^{-9} m²/s, which are about four orders of magnitude smaller than the molecular diffusion of CO₂ in air. An empirical correlation was developed for predicting the effective pore diffusivity with the amount of CO₂ adsorbed and NaOH loading.



Citation: Tangsathitkulchai, C.; Naksusuk, S.; Wongkoblap, A.; Phadungbut, P.; Borisut, P. Equilibrium and Kinetics of CO₂ Adsorption by Coconut Shell Activated Carbon Impregnated with Sodium Hydroxide. *Processes* **2021**, *9*, 201. <https://doi.org/10.3390/pr9020201>

Received: 5 December 2020

Accepted: 15 January 2021

Published: 21 January 2021

Keywords: activated carbon; alkali impregnation; adsorption isotherms; adsorption kinetics; carbon dioxide adsorption

Publisher's Note: MDPI stays neutral with regard to jurisdictional claims in published maps and institutional affiliations.



Copyright: © 2021 by the authors. Licensee MDPI, Basel, Switzerland. This article is an open access article distributed under the terms and conditions of the Creative Commons Attribution (CC BY) license (<https://creativecommons.org/licenses/by/4.0/>).

1. Introduction

Global warming, a slow increase in the average temperature of the earth's atmosphere, has a severe effect on world climate change, which has widespread impacts on humans and ecosystems [1]. This atmospheric warming is caused by the increasing concentrations of greenhouse gases (GHGs) in the upper atmosphere that prevents the dissipation of accumulated heat out into the space [2]. Recent figures show that the greenhouse gases consist of 80% CO₂, 10% CH₄, 7% nitrous oxides, and 3% fluorinated gases [3]. Presently, carbon dioxide (CO₂), the largest contributor to the global warming effect, has the concentration level in the atmosphere of 414 parts per million (ppm), a 47% increase since the beginning of the industrial revolution era in 1750, and still rising at an alarming rate [4]. Carbon dioxide is primarily generated from electricity power plants and large industrial processes (e.g., cement production plants) burning fossil fuels (coal, oil, and natural gas). In 2018, it is estimated that about 38 billion metric tons of CO₂ was released into the atmosphere

from fossil fuel utilization, which accounts for about 50% of total CO₂ emissions from anthropogenic human activities [5]. It is therefore obvious that CO₂ capture at the point source emissions should be the logical means to lower the CO₂ level in the atmosphere, albeit the energy penalties involved in the separation processes are relatively high.

Various processes have been developed for the separation and recovery of CO₂ from flue gas streams using this post-combustion CO₂ capture, such as alkali solvent absorption, adsorption with porous sorbents, membrane separation, and cryogenic distillation [6]. Of these separation processes, CO₂ absorption using amine-based solvents such as monoethanolamine (MEA), diethanolamine (DEA) and methyl-diethanolamine (MDEA) is the most well-established and mature technology and has been widely used especially in natural gas industry for quite a long time, with a reported removal efficiency of as high as 98% [7]. Despite its good performance, there are a number of drawbacks associated with the use of chemical absorption system, including amine degradation through oxidative reactions and thermal degradation, which results in solvent loss and the generation of many toxic substances, such as organic acids, ammonia and amide, amine emissions producing nitrosamines and nitramines, which are harmful to the environment, high corrosiveness of the solvent, and high energy requirement for solvent recovery due to a strong interaction between CO₂ and the alkali solvent [8]. Due to these inherent shortcomings, the removal of CO₂ from a combustion gas mixture using a solid adsorbent, including porous carbon, zeolites, carbon molecular sieves, activated alumina and metal organic framework compounds, has become an attractive alternative as compared to the conventional wet scrubbing process [9]. The main advantages of the adsorption technology for CO₂ capture are the low energy consumption, choices of adsorbent selection, reasonably high adsorption capacity based on a unit mass or a unit volume basis, and easy adsorbent regeneration using the temperature-swing or pressure-swing adsorption processes due to the weak adsorbent-adsorbate interaction forces. For these available adsorbents, activated carbon is one of the most attractive choices for CO₂ removal. It has many favorable characteristics, for example, it has a high surface area and contains a large number of micropores, which help increase the adsorption capacity of CO₂, it is a low cost adsorbent because various agricultural biomass wastes can be used for the preparation, it can be produced with a desirable pore size distribution by controlling the type of precursors and the preparation conditions, it is not sensitive to moisture in the treated gas stream because of the hydrophobic nature of the carbon surface, and the capability of surface chemistry modification for improved adsorption affinity and selectivity [10].

In general, the adsorption performance of activated carbon is governed primarily by its internal pore structure. The pore size distribution and pore connectivity will dictate the diffusion rate (kinetics) of an adsorbate to the adsorption sites, whereas the internal surface area will provide a number of active sites for adsorption to take place. Apart from the effect of pore structure, surface chemistry, due to the presence of various surface functional groups, also plays an important role on the adsorption behavior. Activated carbon mostly contains oxygen functional groups on its surface, which can be acidic or basic functional groups. These functional groups are introduced through the oxidation of defective graphene surfaces containing unpaired electrons and the oxidation of surface heteroatoms such as O, H, S, N, and Cl by the oxidizing gas (CO₂, O₂, or steam) during the activation process [11,12].

Since CO₂ is considered as a weak Lewis acid (electron acceptor), the increase in the basicity of carbon surface which acts as Lewis basic sites (electron donor) would help promote the affinity and selectivity of CO₂ due to a stronger acid-base interaction [13]. Therefore, adsorption capacity of CO₂ by the virgin activated carbon can be further enhanced by increasing the basicity of the carbon surface. This is achieved by treating the activated carbon, for example, by (i) heat treatment in an inert atmosphere at a high temperature (700 °C) to remove the existing surface oxygen functionalities; (ii) chemical treatment to introduce basic functional groups, for example, creating nitrogen functionalities by heating in NH₃ atmosphere at a high temperature range (200–800 °C); and (iii) wet impregnation with

alkali solutions [14,15]. Among these various treatments, the wet impregnation method has received considerable attention because of its simplicity, low cost, and effective CO₂ capture. Various types of alkali impregnation chemicals have been investigated, including K₂CO₃, NaOH, KOH, and ethanolamines. CO₂ adsorption tests using these alkali impregnated carbons were mostly performed in a fixed-bed system [16–21], with an observed increase of up to twofold for CO₂ adsorption capacity, as compared to the case of untreated carbons.

Despite the significance of these surface modified adsorbents, it is surprising that there have been virtually no reports on the study of both equilibrium and kinetics of CO₂ adsorption by alkali impregnated activated carbons. With this impetus, this work was aimed to study and collect information concerning the effect of NaOH impregnation loading in coconut-shell activated carbon on the equilibrium isotherms and kinetic data of CO₂ adsorption from a synthetic flue gas (CO₂+N₂) up to the pressure of about 1 bar. Sodium hydroxide was used as the alkali impregnant in the present study due to the fact that it is relatively cheap and easily obtainable. These isotherm and kinetic data are essential for the successful design of an adsorption system for capturing CO₂ from flue gases at an ambient condition.

2. Theories

2.1. Adsorption Equilibrium Models

In this study, three isotherm models were employed for the analysis of adsorption equilibrium of carbon dioxide by the prepared activated carbons, including Langmuir, Freundlich, and Sips equations. Langmuir equation was first developed for pure gas adsorption on a flat surface based on the concept of dynamic equilibrium or kinetic approach [22]. The assumptions involved are that the adsorption energy is constant irrespective of the amount of gas adsorbed (homogeneous adsorption), adsorption takes place at a definite, localized site, and each site can accommodate only one atom or one molecule, thus leading to the type of monolayer adsorption when all the adsorption sites are fully occupied. The final form of Langmuir equation reads,

$$q_L = \frac{q_m(bP)}{1 + (bP)} \quad (1)$$

where q_L = amount of adsorbate adsorbed (mg CO₂ adsorbed/g activated carbon), q_m = maximum monolayer adsorption capacity (mg/g), b = Langmuir constant or affinity constant, and P = pressure (kPa). Freundlich isotherm is one of the most popularly used empirical equations for describing the adsorption equilibrium data [23]. It was proposed for monolayer adsorption on a heterogeneous surface, that is, the adsorbent-adsorbate interaction energy is distributed and is grouped into patchwise areas with each patch having its own adsorption energy. This equation takes the following form,

$$q_F = K_F(P)^{1/n_F} \quad (2)$$

where q_F = amount of CO₂ adsorbed (mg/g), P = pressure (kPa), K_F = affinity constant and n_F = surface heterogeneity index.

Sips isotherm [24], a three-parameter empirical equation, has the following form,

$$q_S = \frac{q_m(bP)^{1/n_S}}{1 + (bP)^{1/n_S}} \quad (3)$$

where q_S and q_m are in mg/g and P in kPa. This equation is a hybrid model of Langmuir and Freundlich equations, thus showing a characteristic of saturation limit at a high adsorption pressure.

2.2. Adsorption Kinetic Model

The development of a kinetic equation for CO₂ adsorption by activated carbon in this study is obtained by writing a differential mass balance for the diffusion of an adsorbate inside a spherical porous adsorbent [25], as shown in Equation (4).

$$\frac{\partial q}{\partial t} = D_e \left[\frac{\partial^2 q}{\partial r^2} + \frac{2}{r} \frac{\partial q}{\partial r} \right] \quad (4)$$

The solution derived by solving this equation with appropriate initial and boundary conditions in spherical coordinates, that is, $q(r,0) = q(0)$ and $\partial q/\partial r = 0$ at $r = 0$, gives the concentration of adsorbed phase (q) as a function of radial distance (r) and time (t). The derived solution in terms of the fractional uptake (F) is given by Equation (5),

$$F = \frac{q(t) - q(0)}{q_e - q(0)} = 1 - \left(\frac{6}{\pi^2} \right) \sum_{n=1}^{\infty} \left(1/n^2 \right) \exp\left(-\frac{n^2 \pi^2 D_e t}{R_p^2}\right) \quad (5)$$

For the adsorption time close to the equilibrium ($F > 0.7$), we may use only the first term of the summation since the higher terms may be neglected. For this case, the fractional uptake equation takes the form,

$$F = \frac{q(t) - q(0)}{q_e - q(0)} = 1 - \left(\frac{6}{\pi^2} \right) \exp\left(-\frac{\pi^2 D_e t}{R_p^2}\right) \quad (6)$$

In linear form Equation (6) becomes,

$$\ln(1 - F) = \ln\left(6/\pi^2\right) - (\pi^2 D_e t/R_p^2) \quad (7)$$

where $q(t)$ = amount of CO₂ adsorbed at time t (mg/g), $q(0)$ = initial amount of CO₂ adsorbed and is zero for a fresh adsorbent, q_e = amount of CO₂ adsorbed at equilibrium (mg/g), R_p = radius of the spherical adsorbent = 6.45×10^{-4} m for activated carbon particles used in this study, and D_e = the effective or average diffusion coefficient for CO₂ diffusion inside the adsorbent pores (m²/s).

2.3. GCMC Simulation for Gas Adsorption

In this study, we use a Grand Canonical Monte Carlo (GCMC) simulation method to obtain the adsorption isotherms of N₂ and CO₂ in a finite-length slit pore in the presence and absence of NaOH group. Nitrogen is modelled as a spherical Lennard–Jones (LJ) fluid and carbon dioxide is modeled as a 3-center-LJ molecule having LJ interaction sites and point charges, as described in the literature [26,27]. The functional group used in this study is taken as a sodium hydroxide (NaOH) molecule whose model parameters proposed by Santoro et al. [28] is used in this study. The center of the oxygen of the NaOH group is 0.37 nm from the pore wall and perpendicular to the wall. The separation distance between the hydrogen and oxygen atoms is 0.097 nm, and the separation distance between the sodium and oxygen atoms is 0.2072 nm. The angle of Na–O–H is about 119.5°. The solid or adsorbent model is assumed as a slit-shape pore and has three graphene layers constituting a solid wall, as described in the literature [29]. The graphene layers are assumed to be square and equal in size with a linear dimension of 6nm and having a width of 1.5 nm, which is the typical average micropore size observed for activated carbon. The molecular parameters used for the simulation are summarized in Table 1. The interaction forces between two particles (fluid–fluid or fluid–solid molecules) is estimated from the Lennard–Jones 12-6 equation [26,30,31] and the interaction between two charges takes the form of a Coulomb’s law of electrostatic interaction [26]. A cut-off radius of five times the collision diameter of fluid is used in this study.

Table 1. Molecular parameters and atomic partial charges of N₂, CO₂, C, and NaOH used in the Grand Canonical Monte Carlo (GCMC) simulation.

Type	Interacting Site	Collision Diameter, σ [nm]	Reduced Well-depth, ϵ/k_b [K]	Atomic Charge, q [e^-]
N ₂ (Spherical model)	N ₂	0.3615	101.5	0
N ₂ (Multi-site model)	N	0.331	36.0	−0.482
	Center site	0	0	+0.964
CO ₂ (Multi-site model)	C	0.2757	28.129	+0.6512
	O	0.3033	80.507	−0.3256
Activated carbon	C	0.34	28.0	0
	Na	0	0	+0.758
NaOH	O	0.3804	1962	−1.056
	H	0	0	+0.298

In performing the GCMC simulation, we specify the volume of the simulation box, the pressure, or the chemical potential and the temperature of the system to obtain the adsorption equilibrium. One GCMC cycle consists of one thousand displacement moves and attempts of either insertion or deletion with equal probability. For the simulation of adsorption isotherms, two thousand cycles are typically needed for the system to reach equilibrium, and additional 20,000 cycles are used to obtain the ensemble averages. Twenty million configurations are used for equilibration and additional twenty million configurations are used for gathering statistical ensemble. To generate each isotherm point, an empty box without any gas molecule is used as the initial configuration, and the simulation computation is carried out until the number of particles in the box does not change (in statistical sense). The pressure of the bulk gas corresponding to a given chemical potential is calculated from the equation of state proposed by Johnson et al. [32].

2.4. GCMC Simulation for Determining Pore Size Distributions

In this study, we employ the GCMC simulation procedure proposed by Madani et al. [33] and Cornette et al. [34] to obtain the pore size distributions of activated carbon samples. For the determination of pore size distributions from nitrogen isotherms or carbon dioxide isotherms, the following approach is applied. Initially, a set of 50 unit cells consisting of a graphitic surface and 49 slit carbon pores with different physical pore sizes (H_i) ranging from 0.60 to 3 nm are constructed and the solid-fluid interaction is modeled with Steele 10-4-3 walls [35]. To simulate the gas adsorption in the micropores of activated carbon, the slit pore model with different pore sizes (H_i) varying from 0.60 to 3 nm (with 49 unit cells having equal spacing of 0.05 nm) are specified to cover the entire micropore size range. The fluid-fluid interaction force of nitrogen and that of carbon dioxide are considered as multi-site model [34], as shown in Table 1. Two Lennard-Jones sites and three Coulombic sites are for nitrogen-nitrogen interaction, while the interaction of carbon dioxide molecules is modelled as three Lennard-Jones sites and three Coulombic sites [36]. Once the unit cells are set, 50 local isotherms are then calculated using grand canonical Monte Carlo simulation (GCMC) for nitrogen adsorption at 77 K or carbon dioxide adsorption at 273 K. Each adsorption isotherm consists of 100 pressure points to cover the range of relative pressure (P/P^0) from 1×10^{-4} to 1. The general procedure for GCMC computation is as follows. The linear dimension of simulation box is $5 \times 5 \text{ nm}^2$ with periodic boundary conditions being applied in those directions, and the cut-off radius is considered half of the box length. In this GCMC simulation, 100,000 cycles are used in both the equilibration and sampling stages. Each cycle consists of 1000 Monte Carlo moves with equal probabilities for local displacement move, insertion, and deletion based on the conventional Metropolis

rules. Therefore, 1×10^8 configurations in total are conducted to simulate the adsorption isotherm. At the initial stage, a collection of local adsorption isotherms is obtained for different pore sizes of carbon slit pores. The adsorbed density is expressed as the absolute adsorbed amount in the pore per unit accessible volume ($\rho_{A,i}$), while for the surface model the density is represented as the excess amount per unit surface area (Γ_{ex}). The porous characterization of activated carbon is then determined using the mass balance method [35], for which the total number of particles introduced in the adsorption cell is defined as

$$N = \rho_g V_g + S_{ext} \Gamma_{ex} + \sum_{i=1}^M v_{A,i} \rho_{A,i} \quad (8)$$

where the first, second, and third terms in the right-hand side of the equation are the number of particles in the gas phase, on the surface and in the pores of adsorption cell and ρ_g is the bulk gas density.

Analogous to the adsorption integral approach, the experimental N_2 and CO_2 isotherms of activated carbons and local isotherms of simulated models are then matched by means of Monte Carlo optimization to minimize the mean square error and root-mean-square deviation between experimental isotherms and the isotherms calculated from Equation (8). The obtained results are the accessible pore volume for each pore size ($v_{A,i}$), external surface area (S_{ext}) and volume of gas phase in the adsorption cell (V_g). Finally, the derived pore size distribution (PSD) of activated carbon is presented as the relationship between the differential pore volume per unit pore width ($dv_{A,i}/H_{A,i}$) and the average pore width ($\bar{H}_{A,i}$).

3. Experimental Method

3.1. Materials

Activated carbon used in this study, having an average screen size of 1.29 mm, was commercially produced from coconut shell by steam activation and supplied by C. Gigantic Carbon Co., Ltd. in Nakhon Ratchasima Province, Thailand. Two types of activated carbon with BET (Brunauer-Emmett-Teller) surface areas of $766 \text{ m}^2/\text{g}$ (designated as AC1) and $1052 \text{ m}^2/\text{g}$ (designated as AC2), were employed for the CO_2 adsorption tests. Nitrogen gas (N_2) and carbon dioxide gas (CO_2) of high purity (99.99%) were purchased from Linde Thailand. Sodium hydroxide in powder form of form of AR (analytical reagent) grade was purchased from Carlo Erba Reagents.

3.2. Preparation of NaOH Impregnated Activated Carbon

For each batch of preparation, 50 g of the original activated carbon was mixed with 180 cm^3 of NaOH solution of the desired concentration (3–15 wt% NaOH). The mixture was shaken in a temperature-controlled water bath at $25 \text{ }^\circ\text{C}$ using a shaking speed of 100 rpm for 120 min to attain the equilibrium condition. After that, the whole suspension was dried in an electric oven at $110 \text{ }^\circ\text{C}$ for 48 h. With this method of total alkali impregnation, it is clear that at a low NaOH concentration most of NaOH will reside inside the adsorbent pores resulting from mass diffusion. As the concentration is progressively increased, NaOH will distribute both inside the pores and at the external surfaces of the activated carbon, leading eventually to the blocking of the pore entrance at a very high NaOH concentration. It is noted that this impregnation technique is simple and more practical but the equilibrium adsorption isotherm of NaOH (the equilibrium relationship between the concentrations of NaOH in the solution and in the adsorbed phase) cannot be directly obtained, unless the suspension is filtered out and the concentration of NaOH determined. The corresponding amount of NaOH being adsorbed in the adsorbent pores at equilibrium is then calculated from the initial and final NaOH concentrations.

3.3. Measurement of Carbon Porous Properties

Porous properties of the original activated carbon and activated carbon impregnated with NaOH were determined from the measured N₂ adsorption isotherms at 77 K, using a surface area and pore analyzer (ASAP2020, Micromeritics, Norcross, GA, USA). The BET and Langmuir surface areas were calculated from the N₂ isotherms using the BET equation and the Langmuir theory, respectively, and the micropore volume was computed from the t-plot theory [37,38]. The total pore volume was determined by converting the volume of N₂ gas adsorbed at the relative pressure (P/P°) of 0.98 into the corresponding volume of nitrogen in liquid state at 77 K, that is, to assume that nitrogen is adsorbed as a liquid-like fluid in the narrow pores of the activated carbon due to a strong force field between pore walls. The mesopore volume was derived by subtracting the micropore volume from the total pore volume. The average pore size was calculated from the equation $4V/A$, where V and A are the total pore volume and BET surface area, respectively, assuming a cylindrical-shaped pore. The pore size distribution of activated carbon was derived from the GCMC simulation method as described in Section 2.4.

3.4. Study of Equilibrium and Kinetics of CO₂ Adsorption

The study of adsorption equilibrium and kinetics of carbon dioxide by the original and NaOH impregnated activated carbons was carried out using the surface area and pore analyzer (ASAP2020, Micromeritics, Norcross, GA, USA) by measuring the amounts of CO₂ adsorbed as a function of increasing pressure at 273 K (0 °C). The carbon sample of 0.25 g was loaded into the sample tube and degassed at the temperature of 573 K (300 °C) and the pressure of 1.3 kPa (0.0013 bar) for 720 min to remove any impurities remaining in the pores of the adsorbent. Next, the sample tube was transferred to the measurement port for collecting the adsorption data at a constant temperature. The sample was first dosed with a certain volume of CO₂ and the amount of CO₂ adsorbed was then recorded as a function of time until the equilibrium was attained, that is, the constant amount of CO₂ adsorbed and the constant system pressure were finally obtained. This measurement was performed for a series of increasing CO₂ dosage until the final equilibrium pressure reached approximately one bar, which is the maximum pressure limit of the instrument. About 100–150 data points of adsorbed amount vs time for each equilibrium pressure were obtained for each carbon samples tested. Data of the amount adsorbed versus time during the adsorption kinetic measurement were used for the analysis of adsorption kinetics, whereas the relationship between the amount adsorbed at the equilibrium and the equilibrium pressure gave the adsorption isotherm information.

4. Results and Discussion

4.1. N₂ Isotherms of Original and Alkali Impregnated Activated Carbons

Figure 1 shows N₂ adsorption-desorption isotherm curves of the original and NaOH impregnated activated carbons at 77 K and the relative pressure (P/P°) ranging from 0 to 1. It is clear that all isotherms exhibited Type I isotherm based on IUPAC (International Union of Pure and Applied Chemistry) classification [38], which is characterized by a rapid increase in the amount of gas adsorbed over relatively low pressures, and followed by a plateau region at higher pressures. This isotherm behavior signifies that the tested activated carbons contain mostly micropores with the pore sizes smaller than 2 nm and the adsorption taking place by the pore-filling mechanism [39]. There are small hysteresis loops associated with the isotherms and the size of the loops tended to decrease with the increase of NaOH loading. It is noted that the size of a hysteresis loop is indicative of the relative volume of mesopores in the activated carbon; the larger the size of the hysteresis loop, the larger the proportional volume of the mesopores. In addition, at the same pressure, the amounts of N₂ adsorbed for AC2 series were higher than those of the AC1 series, which are ascribed to the larger surface areas of AC2, as compared to that of AC1, and the adsorbed amount of N₂ appeared to decrease with the increase of NaOH impregnation loading. This last notion will be examined further in the next section.

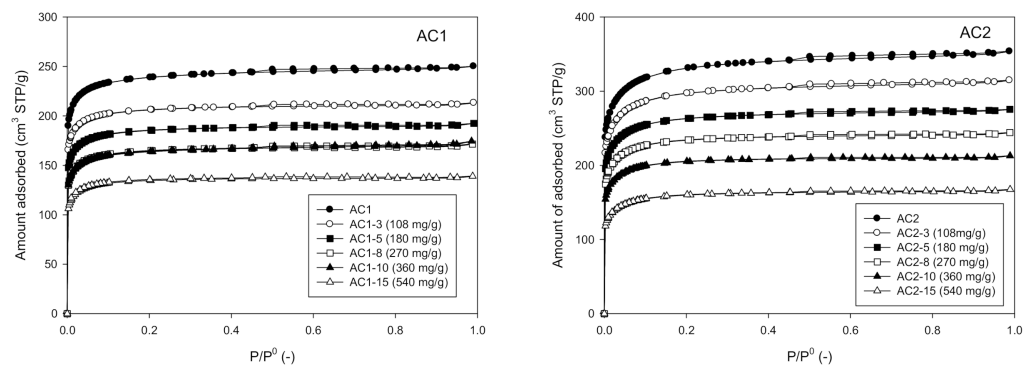


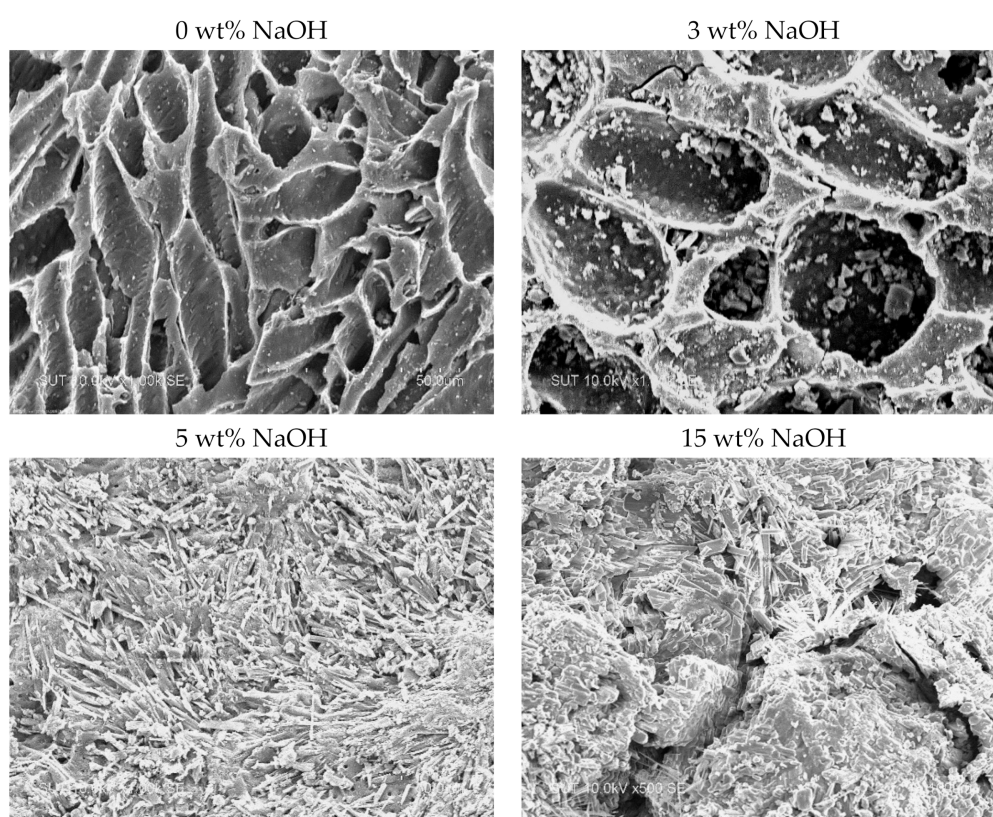
Figure 1. Effect of NaOH impregnation loading on N₂ adsorption isotherms measured at 77 K for AC1 and AC2 original activated carbons.

4.2. Porous Properties of the Original and Alkali Impregnated Activated Carbons

Table 2 shows porous properties of the tested activated carbons, as computed from the N₂ adsorption isotherms at 77 K. The surface area calculated by the Langmuir equation, which is suitable for Type I isotherm, was consistently about 37% higher than the surface area calculated from the BET equation, which is generally applied to the Type II isotherm for the relative pressures (P/P^0) of less than about 0.3 [40,41]. It is observed that both the surface area and total pore volume decreased continuously by about 48% as the NaOH loading was increased from 0 to 540 mg/g. It is anticipated that eventually all the internal pores will be completely blocked at a very high loading of NaOH. In principle, this maximum amount of NaOH loading could be estimated from the total pore volume and the state of molecular packing of NaOH inside the pores of activated carbon. Table 1 further reveals that the average pore size tended to decrease with the increase of NaOH loading, but the effect is not so pronounced, being less than about 3%. To observe the effect of NaOH loading on the morphology of activated carbon surface, the SEM images of AC2 activated carbon are shown in Figure 2 for increasing concentrations of NaOH solution used for the impregnation. The porous nature of surface can be seen for the original activated carbon with the absence of sodium hydroxide particles. At 3 wt% concentration, the appearance of some NaOH particles residing inside the pores is discernible, indicating that most of NaOH particles are present inside the internal pores. At a higher concentration of 5 wt% NaOH, the deposited layer of NaOH appears to cover the outer surface but still with the appearance of some small pore openings at the carbon surface. At a very high concentration of 15 wt%, the external surface is completely covered by the thick layer of deposited NaOH particles. To check for the presence of NaOH in activated carbon, a SEM-EDX (Scanning Electron Microscopy with Energy Dispersive X-ray) instrument (model JSM-7800F, JEOL, Tokyo, Japan) was employed for the analysis of elemental identification and quantitative compositions of the activated carbon samples. As an example, the results of SEM images, elemental spectra and X-ray maps are presented in Figure 3 for the AC2-3 sample and Table 3 shows the concentrations of carbon, oxygen and sodium atoms for AC2, AC2-3, AC2-5, and AC2-15 samples. It should be noted that the hydrogen atom is too small to be detected by the EDX technique. The spectra indicated the peak of a carbon atom that should belong to the graphene structure of activated carbon, while the peaks of sodium and oxygen atoms should represent those of the sodium hydroxide molecule. The distribution of sodium and oxygen atoms on the background of carbon surface is highlighted by the X-ray-mapping results for the AC2-3 sample. It is further observed from Table 3 that the atomic % of sodium and oxygen also increased with the concomitant increase of weight % NaOH solution used for the impregnation, as would be expected.

Table 2. Porous properties of the original and NaOH impregnated activated carbons.

Sample	NaOH Concentration (wt%)	NaOH Loading (mg/g)	Langmuir Surface Area (m ² /g)	BET Surface Area (m ² /g)	Micropore Volume (cm ³ /g)	Mesopore Volume (cm ³ /g)	Total Pore Volume (cm ³ /g)	Average Pore Diameter (nm)
AC1	0	0	1055	766	0.375 (96.9%)	0.012 (3.1%)	0.387	0.202
AC1-3	3	108	908	663	0.324 (98.2%)	0.006 (1.8%)	0.330	0.199
AC1-5	5	180	817	596	0.291 (98.0%)	0.006 (2.0%)	0.297	0.200
AC1-8	8	270	726	529	0.259 (97.7%)	0.006 (2.3%)	0.265	0.200
AC1-10	10	360	723	527	0.257 (95.2%)	0.013 (4.8%)	0.270	0.205
AC1-15	15	540	593	433	0.212 (98.6%)	0.003 (1.4%)	0.215	0.199
AC2	0	0	1477	1052	0.393 (71.8%)	0.154 (28.2%)	0.547	0.208
AC2-3	3	108	1150	841	0.330 (78.6%)	0.090 (21.4%)	0.420	0.203
AC2-5	5	180	1137	827	0.319 (77.6%)	0.092 (22.4%)	0.411	0.203
AC2-8	8	270	1022	750	0.297 (80.3%)	0.073 (19.7%)	0.370	0.201
AC2-10	10	360	907	659	0.264 (80.2%)	0.065 (19.8%)	0.329	0.200
AC2-15	15	540	709	514	0.198 (76.4%)	0.061 (23.6%)	0.259	0.201

**Figure 2.** SEM images of coconut-shell activated carbon (AC2) impregnated with NaOH solutions of varying concentrations.**Table 3.** Elemental compositions of NaOH impregnated activated carbons obtained from SEM-EDX (Scanning Electron Microscopy with Energy Dispersive X-Ray) analysis.

Samples	C		O		Na	
	Wt%	Atomic%	Wt%	Atomic%	Wt%	Atomic%
AC2	92.18	94.01	7.82	5.99	-	-
AC2-3	45.20	53.92	43.77	39.20	11.03	6.88
AC2-5	36.52	45.06	49.80	46.13	13.67	8.81
AC2-15	15.34	20.95	59.81	61.32	24.85	17.73

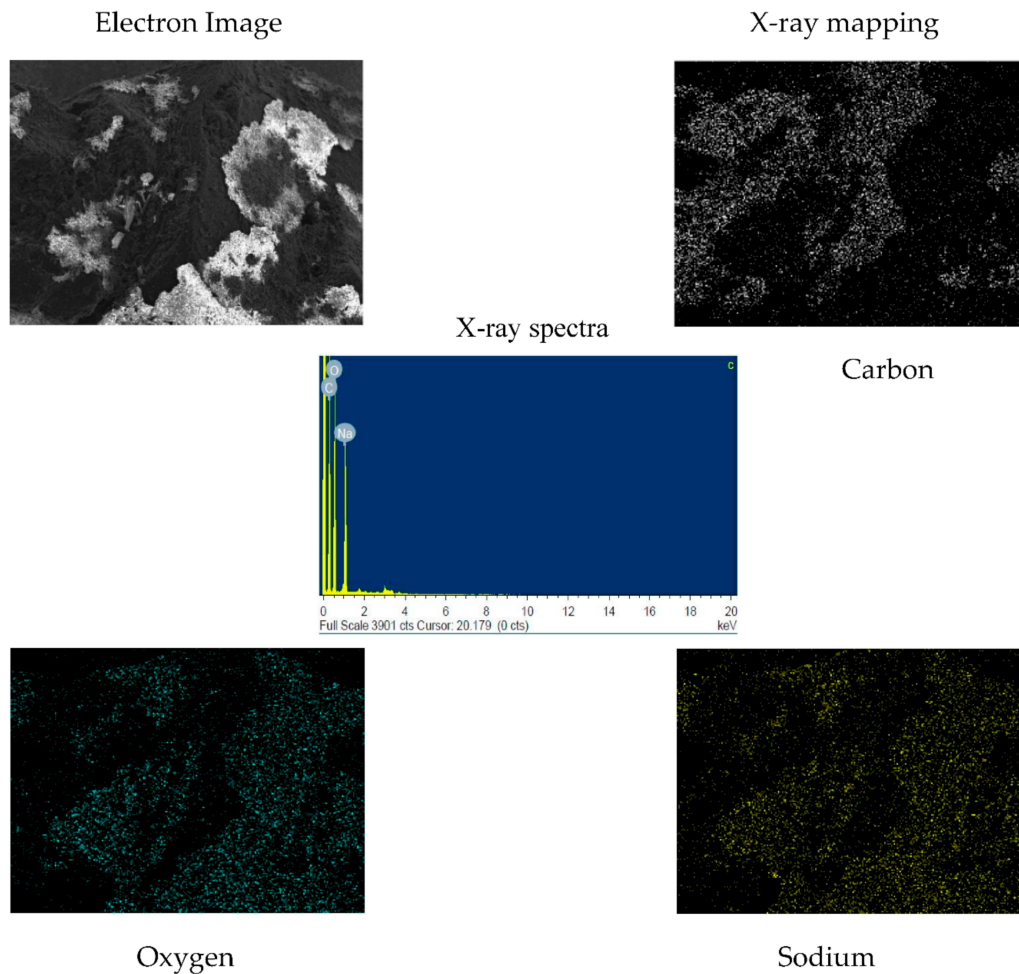


Figure 3. Results of SEM-EDX analysis of NaOH impregnated activated carbons (AC2-3 sample).

It is interesting to understand the reason why the amount of N_2 adsorbed, and, hence, the porous properties of activated carbon, tended to decrease with the increasing amount of NaOH impregnation. There are two likely effects, relating to the adsorbent-adsorbate affinity, which could be responsible for this adsorption behavior. For the first effect, N_2 could adsorb onto the NaOH sites and the increasing amount of NaOH would lead to the reduction of volume of the pore space, thus giving less amount of N_2 being adsorbed in the remaining available pore space. The second effect could be related to the low affinity of N_2 towards NaOH adsorption sites. In other words, N_2 molecules can only adsorb onto the carbon surface. Therefore, the free surface area available for adsorption diminishes as the amount of NaOH depositing on the surface is increased, leading also to a decrease in the adsorbed amount of N_2 inside the pores.

The first effect was proved by applying the grand canonical Monte Carlo (GCMC) simulation to examine the adsorption behavior of N_2 at 77 K in the slit-pore model with the presence of NaOH active sites. Figure 4 shows typical snapshots of nitrogen adsorption in the finite-length pores of 1.5 nm in width, with the presence of NaOH molecules at increasing pressures from 10 to 10^5 Pa. A rather strong interaction between N_2 molecules and NaOH can be observed. The formation of two adsorbed layers along the pore surface and one layer at the pore center at 10 Pa pressure can be noticed. At higher pressures, three layers of adsorbed nitrogen can be clearly seen. Next, the accessible pore volume, which is defined as the remaining pore volume available for N_2 adsorption excluding the volume of occupying NaOH molecules, was calculated based on the GCMC simulation as a function of NaOH concentration (number of NaOH molecules on the slit-pore surfaces) and the calculated results are presented in Table 4. The accessible pore volume did drop

continuously as the number of NaOH molecules increased, with a reduction by almost 100% as the number of NaOH molecules was increased to 689 molecules. From the GCMC simulation results, it can thus be inferred that N₂ molecules showed a relatively strong affinity with NaOH adsorption sites and the reduction of the amounts of N₂ adsorbed with the increase of alkali loading is clearly caused by the consequent decrease of the pore volume available for N₂ adsorption. As a result of this evidence, the second hypothesis of low affinity of N₂ towards NaOH adsorption sites should be disregarded.

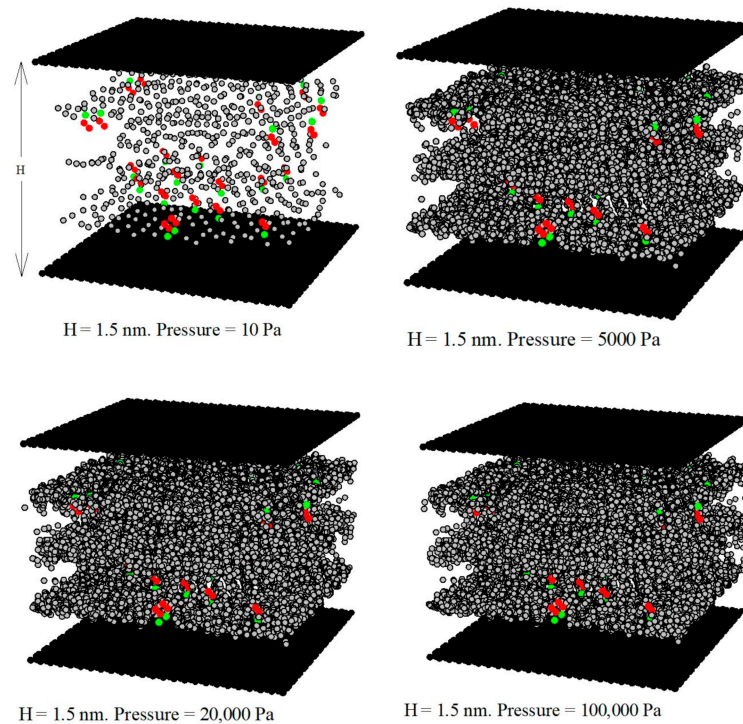


Figure 4. Snapshots from GCMC simulation showing the adsorption of nitrogen molecules onto the randomly distributed NaOH molecules on the graphene surface of the slit pore model of activated carbon for various increasing adsorption pressures (green spheres, red spheres, and gray spheres represent Na atoms, OH groups, and nitrogen molecules, respectively).

Table 4. Accessible pore volume for CO₂ adsorption as a function of NaOH loading in a pore of 1.5 nm in width, computed from GCMC simulation.

Total Pore Volume = 1143 cm ³ /g			
No. of NaOH Molecules on the Graphene Surface	%NaOH Molecules Relative to Total no. of Carbon Atoms at Two Opposite Walls	Accessible Pore Volume (cm ³ /g)	%Volume Reduction
3	0.1	1117	2.3
17	0.6	1077	5.8
31	1.0	964	15.7
89	3.0	711	37.8
138	5.0	477	58.3
278	10.0	275	75.9
419	15.0	171	85.0
689	25.0	26	97.7

The effect of NaOH loading on the adsorption of N₂ was further examined by determining the pore size distribution (PSD) of the impregnated activated carbons, using the GCMC simulation method as outlined in Section 2.4. The pore size distributions obtained from the GCMC simulation are displayed in Figure 5 and Figure 6 for AC1 and AC2 acti-

vated carbons impregnated with NaOH, respectively. The results show a multimodal pore size distribution, consisting of five pore size intervals, 0.6–0.9 nm (denoted as range A), 0.9–1.2 nm (B), 1.2–1.5 nm (C), 1.5–1.8 nm (D), and 1.8–2.0 nm (E), with the pore size range of 1.2–1.5 nm possessing maximum pore volume. The percentage volume of this pore size range varied from 28.5–44.5% and 28.5–40.6% for AC1 and AC2 series, respectively, depending on the amount of impregnated NaOH. It can be observed that the increase in the amount of alkali impregnation tended to lower the pore volume of all pore sizes in varying degrees, which supports the hypothesis of pore volume reduction effect, as discussed earlier.

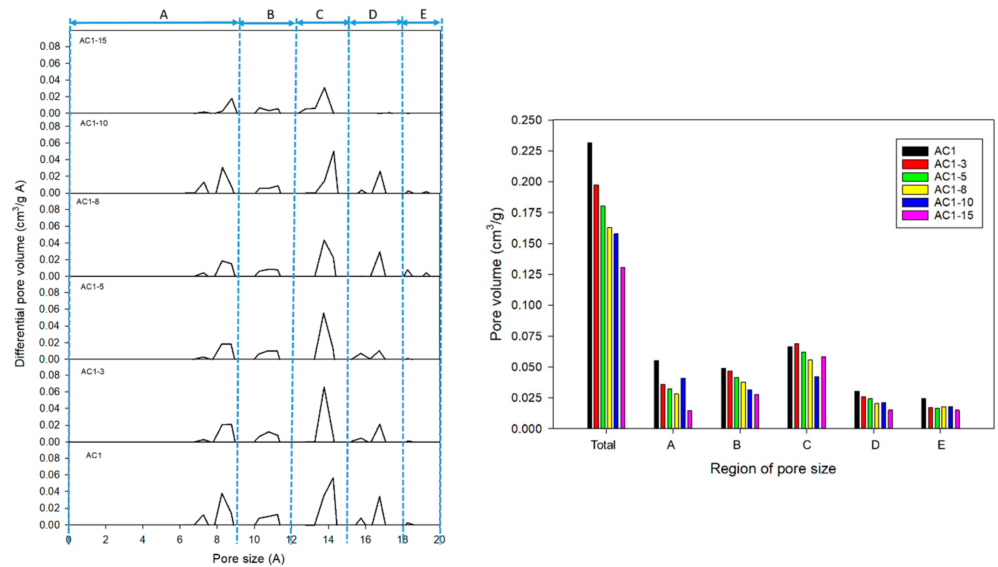


Figure 5. Effect of NaOH loading on the pore size distribution and local pore volume of NaOH impregnated activated carbons AC1, computed by the GCMC simulation using N_2 as a probe molecule.

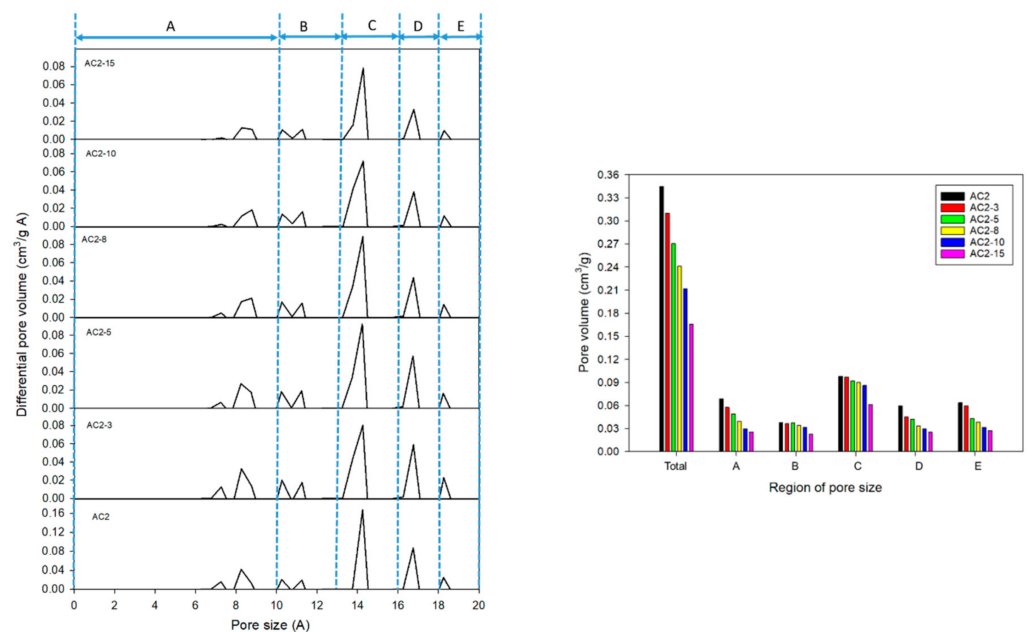


Figure 6. Effect of NaOH loading on the pore size distribution and local pore volume of NaOH impregnated activated carbons AC2, computed by the GCMC simulation using N_2 as a probe molecule.

4.3. Equilibrium of CO₂ Adsorption

Figure 7 shows the equilibrium adsorption isotherms of CO₂ at 273 K (0 °C) by coconut-shell activated carbon impregnated with sodium hydroxide solution of varying concentrations from 0–15 wt%, corresponding to the NaOH loading from 0–540 mg NaOH/g carbon, for the pressure range up to about 100 kPa (about 1 bar). Since almost all the pores of the original and alkali impregnated activated carbons are in the micropore size range of smaller than about 2 nm; thus, the adsorption of CO₂ in a low pressure range of less than 100 kPa, corresponding to the relative pressure of 0.03, will occur in a very narrow pores of size possibly two to three times larger than the molecular size of CO₂. Figure 7 shows that the amount of CO₂ adsorbed increased with the increase of pressure with the adsorption taking place in the smallest pores first at low pressures and progressing to the next larger pore sizes by the pore-filling mechanism at higher pressures. Therefore, the shape of the isotherm curves in Figure 7 represents the initial part of Type I isotherm, according to the IUPAC classification [38]. Figures 8 and 9 show typical snapshots from GCMC simulation of carbon dioxide adsorption obtained in finite length pores of 1.5 nm width in the presence and absence of NaOH molecules at 273 K. At the same pressure, the amount of CO₂ adsorbed with the presence of NaOH was obviously greater than that for the case of without NaOH, indicating a stronger interaction between CO₂ and NaOH as compared to the interaction between CO₂ and the carbon surface. Figure 10 shows the effect of temperature (0–30 °C) on CO₂ adsorption isotherms. It is clear that the amount of CO₂ adsorbed tended to decrease with the increase of adsorption temperature for both the original activated carbon (AC2) and activated carbon impregnated with NaOH (AC2-5). This indicates that the adsorption of CO₂ in activated carbon is by physical adsorption involving the dispersive intermolecular forces.

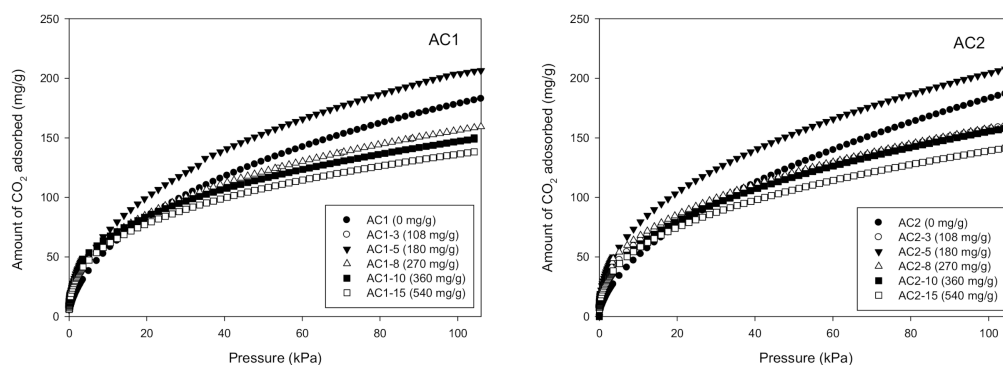


Figure 7. Isotherms of CO₂ adsorption at 273 K by coconut shell activated carbons, AC1 and AC2, impregnated with different amounts of sodium hydroxide (saturation pressure of CO₂ at 273 K is 3500 kPa).

To clarify the effect of NaOH loading on the adsorption behavior of CO₂, the amounts of CO₂ adsorbed from the isotherms in Figure 7 were cross-plotted as a function of the amount of impregnated NaOH in the unit of mg NaOH/g adsorbent for various pressures, as shown in Figure 11. It is seen that NaOH loading showed a definite effect on the adsorption of CO₂. Consider first the effect of increasing NaOH loading from 108 to 540 mg/g, it was found that the adsorbed amount of CO₂ increased with the increasing amount of impregnated alkali and passed through a maximum at an optimum alkali loading of 180 mg/g (5 wt% NaOH) for both the AC1 and AC2. At the maximum pressure of 100 kPa (1 bar), the maximum CO₂ adsorption were 205.8 and 206.1 mg/g, respectively, for AC1 and AC2 impregnated with 180 mg NaOH/g carbon. At the same pressure of 1 bar, the amounts of CO₂ adsorbed by the original activated carbons AC1 and AC2 were 181.2 and 184.6 mg/g. Therefore, the percentage increase of CO₂ adsorption for the alkali impregnated carbon compared to the original carbon was found to be 13.6 and 11.6% for AC1 and AC2, respectively.

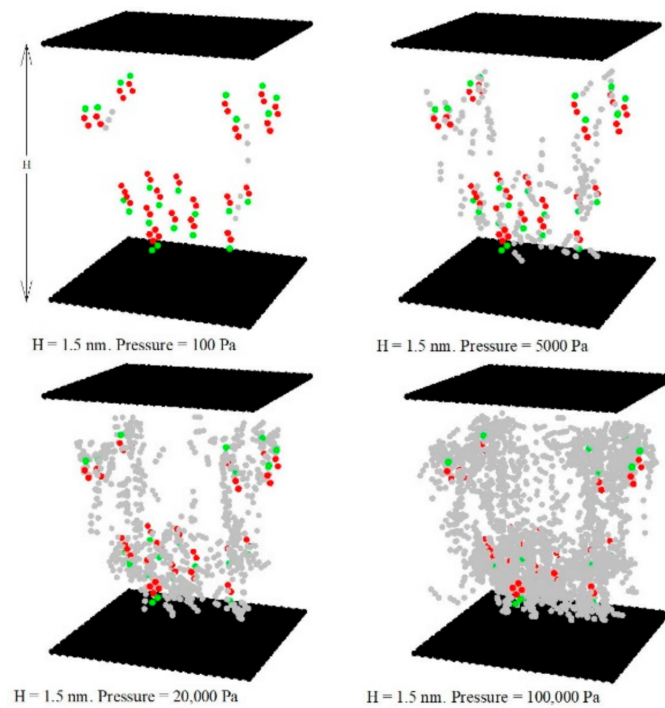


Figure 8. Snapshots of carbon dioxide adsorption at 273 K in pores of width 1.5 nm with the presence of NaOH molecules for various pressures, 100, 5000, 20,000, and 100,000 Pa. (green spheres, red spheres, and gray spheres represent Na atoms, OH groups, and carbon dioxide molecules, respectively).

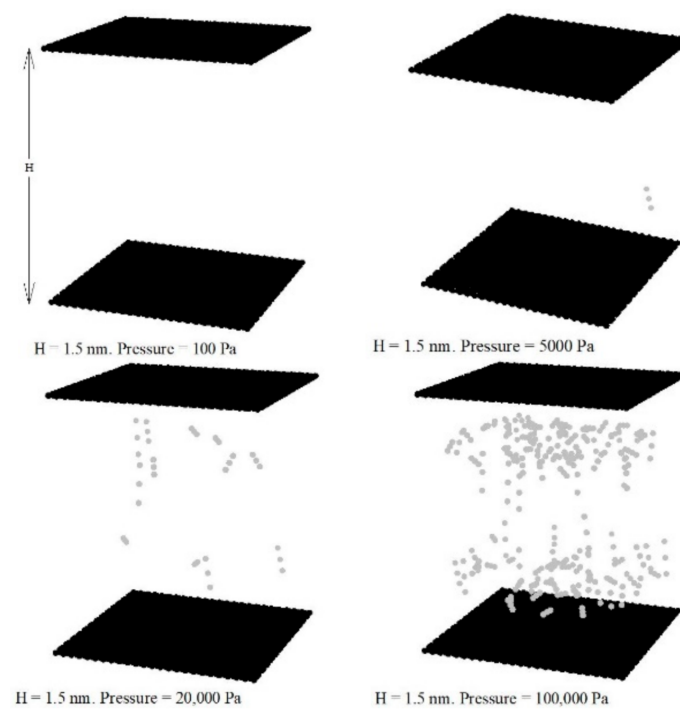


Figure 9. Snapshots of carbon dioxide adsorption at 273 K in pores of width 1.5 nm without the presence of NaOH molecules for various pressures, 100, 5000, 20,000, and 100,000 Pa (gray spheres represents carbon dioxide molecules).

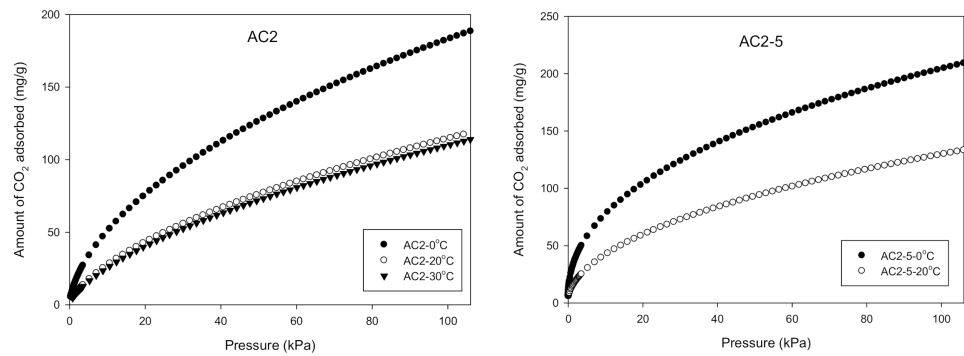


Figure 10. Effect of temperature on CO₂ adsorption of AC2 and AC2-5 samples.

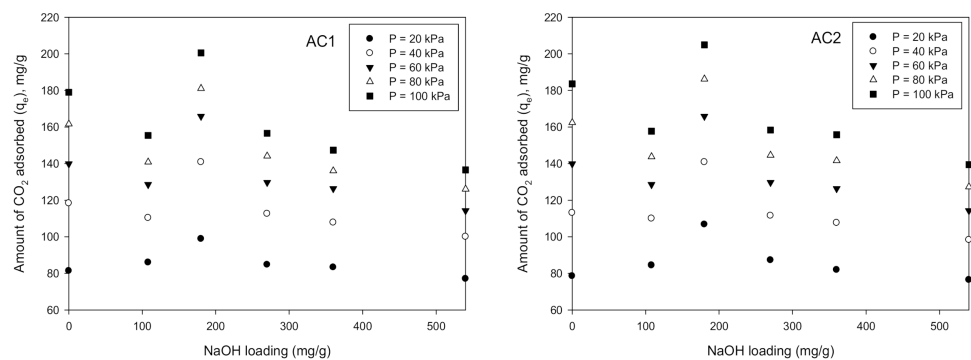


Figure 11. Effect of NaOH loading on the amount of CO₂ adsorbed by coconut shell activated carbon (AC1 and AC2) at various pressures.

The occurrence of the optimum NaOH loading can be explained by the competitive effect between the rate of CO₂ transport through pores (mass transfer resistance) and the ability of CO₂ to interact with the adsorption sites (adsorption affinity). For NaOH loadings lower than the optimum loading of 180 mg/g, the pore size is still sufficiently large in relation to the molecular size of CO₂, thus giving no restriction on the transport rate of CO₂ to the adsorption sites. Therefore, in this regime the amount of CO₂ adsorption is controlled solely by the interaction between CO₂ molecules and the adsorption sites. For this reason, increasing the amount of NaOH will provide the increasing number of adsorption active sites, thus allowing more adsorption of CO₂ to occur. However, at NaOH loadings larger than the optimum NaOH loading, the mass transfer resistance comes into effect and becomes the rate-determining step because of the narrowing of the pores, caused by the increasing amount of depositing NaOH molecules. As a result of this pore restriction effect, the rate of CO₂ transport to the adsorption sites, and hence the amount of CO₂ adsorbed at equilibrium, diminishes continuously as the NaOH loading increases. It is further noticed from Figure 11 that the amount of CO₂ adsorbed at NaOH loading of 108 mg/g (3 wt% NaOH) was lower than that of the original unmodified activated carbon. This indicates that the alkali addition for increased CO₂ adsorption seems to be beneficial only when an optimum alkali loading is used, which in turn depending on the porous structure of the activated carbon employed. From this finding, it may be worthwhile to synthesize activated carbon containing a larger proportion of mesopores so that a larger amount of NaOH could be added into the pores, thus possibly enabling the increasing amount of adsorbed CO₂.

Figure 12 shows pore size distributions of AC2 series determined from GCMC simulation and experimental CO₂ isotherms at 273 K. As seen, the pore size distributions consist of several pore size intervals ranging from around 0.7–2.2 nm. It is clear that most of the adsorption occurs in the smallest pore size range of 0.7–0.9 nm, due principally to

the strong interaction potential in the very narrow pores. This pore size can be compared with the optimal pore size of 0.8 nm for maximum CO₂ adsorption by phenolic resin-based activated carbon spheres [42,43], or with GCMC simulation of CO₂ adsorption that predicted the highest adsorption density for 0.4 nm slit pores [44].

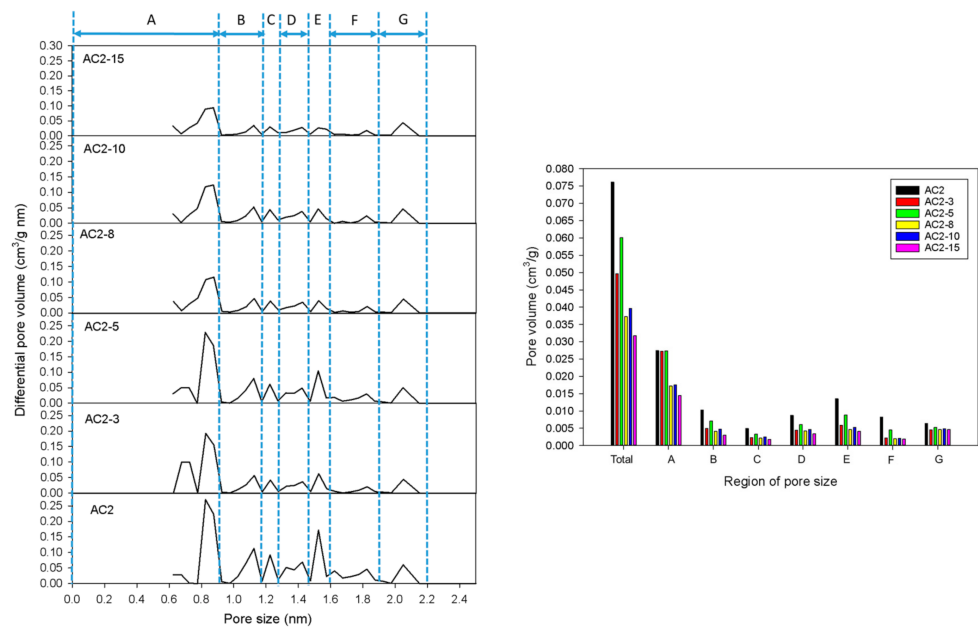


Figure 12. Pore size distributions of the original and NaOH impregnated AC2 derived from CO₂ adsorption isotherms at 273 K and computed by Monte Carlo optimization and mass balance method.

Next, the experimentally measured CO₂ isotherms at 273 K of the tested activated carbons (AC1 and AC2) were compared with those computed from the isotherm models of Langmuir, Freundlich and Sips and a non-linear regression analysis was applied to obtain the best set of model parameters by minimizing the sum square error (SSE) between the experimental and the calculated isotherms. Table 5 shows the derived parameters of the three adsorption models. Based on the values of regression coefficient (R^2), the isotherms were best described by Sips equation, followed by Freundlich and Langmuir equations, respectively. Since the two-parameter Freundlich equation gave model prediction equally well as compared with the three-parameter Sips equation, it is therefore more convenient to use the Freundlich equation for predicting CO₂ adsorption isotherms for the alkali impregnated activated carbons in this study. The variation of affinity parameter (K_F) of Freundlich equation with NaOH loading for both the AC1 and AC2 followed the same trend as that of the amount of CO₂ adsorbed (Figure 11), with the maximum of K_F value occurring at the same optimum NaOH loading of 180 mg/g (5 wt% NaOH). There was a tendency for the surface heterogeneity parameter (n_F) to increase over a narrow range from 1.79 to 2.77 for the increase of NaOH loading from 0 to 540 mg/g for both types of activated carbons. The increasing value of n_F is indicative of increasing degree of surface heterogeneity (wider distribution of adsorption energy) as the number of NaOH adsorption sites increases.

Table 5. Fitted parameters of isotherm equations for CO₂ adsorption at 273 K by the original and NaOH impregnated activated carbons.

Samples	NaOH Loading (mg/g)	Langmuir			Freundlich			Sips			
		q _m (mg/g)	b	R ²	K _F	n _F	R ²	q _m (mg/g)	b	n _S	R ²
AC1	0	237	0.027	0.99	17.7	1.98	0.99	517	3.64 × 10 ⁻³	1.58	1.00
AC1-3	108	148	0.138	0.92	26.8	2.62	0.99	7388	4.66 × 10 ⁻⁷	2.60	0.99
AC1-5	180	245	0.038	0.98	27.8	2.30	0.99	4365	1.16 × 10 ⁻⁵	2.24	0.99
AC1-8	270	170	0.061	0.97	26.3	2.58	0.99	886	2.81 × 10 ⁻⁴	2.32	1.00
AC1-10	360	152	0.081	0.96	27.8	2.75	0.99	728	3.47 × 10 ⁻⁴	2.44	0.99
AC1-15	540	141	0.082	0.96	26.1	2.77	0.99	796	1.91 × 10 ⁻⁴	2.51	1.00
AC2	0	272	0.019	0.99	14.1	1.79	0.99	955	1.01 × 10 ⁻³	1.59	0.99
AC2-3	108	176	0.051	0.96	24.6	2.48	1.00	2447	1.67 × 10 ⁻⁵	1.39	0.99
AC2-5	180	235	0.045	0.97	29.9	2.39	0.99	4126	1.03 × 10 ⁻⁵	2.33	0.99
AC2-8	270	170	0.062	0.96	26.5	2.58	0.99	1291	2.59 × 10 ⁻⁵	2.41	0.99
AC2-10	360	178	0.046	0.97	22.8	2.39	0.99	2387	2.14 × 10 ⁻⁵	2.31	0.99
AC2-15	540	151	0.060	0.96	23.6	2.59	1.00	2550	7.61 × 10 ⁻⁶	2.52	0.99

Attempt was made to correlate the affinity constant (K_F) and the heterogeneity index (n_F) of the Freundlich isotherm equation with the type of activated carbon (AC1 and AC2) in terms of BET surface area (m²/g) of the original activated carbons and NaOH loading (mg/g), using the polynomial function. The empirical equations obtained, for CO₂ adsorption at 273 K, are as follows.

$$K_F = 0.462 + 1.53 \times 10^{-3}X_2 - 6.59 \times 10^{-8}X_1^2 - 2.20 \times 10^{-6}X_2^2 - 1.11 \times 10^{-7}X_1X_2, R^2 = 0.6847 \quad (9)$$

$$\text{and } n_F = 2.13 + 3.66 \times 10^{-3}X_2 - 1.55 \times 10^{-7}X_1^2 - 3.51 \times 10^{-6}X_2^2 - 6.38 \times 10^{-7}X_1X_2, R^2 = 0.7297 \quad (10)$$

where X₁ = BET surface area of the original activated carbons in the range from 766–1052 m²/g, X₂ = amount of NaOH loading in the range from 0–540 mg/g

The proposed correlation for K_F is less satisfactory than that of n_F. The maximum error and the average error are 21.6 and 8.8%, and 0.107 and 0.05% for the prediction of K_F and n_F, respectively.

4.4. Kinetics of CO₂ Adsorption

Figure 13 shows typical kinetic data collected during the transient measurement of CO₂ adsorption at 273 K by activated carbon, in terms of CO₂ uptake versus adsorption time for various increasing pressures. For each pressure, the amount of CO₂ adsorbed increased with increasing time and finally approached an equilibrium adsorbed amount (q_e). For each equilibrium pressure, the adsorption kinetic data (F vs. t) were fitted with Equation (5) using the non-linear regression to obtain the value of effective diffusivity (D_e). SCILAB, a free and open source software, was used in this study for the regression analysis. Since Equation (5) gives the solution of the fractional uptake (F) as infinite series, the approximate number of terms (n) in the summation must be chosen to facilitate the regression.

Figure 14 typically shows that there was virtually no change in the computed diffusivity when using the number of summation terms in Equation (5) larger than 3 (n > 3). Therefore, the effective diffusivity for all the kinetic data were computed via Equation (5) using only three terms in the summation. It was noted that the average regression coefficient (R²) for fitting all the experimental kinetic data of CO₂ adsorption by the pore diffusion model was found to be about 0.987. With the aid of the Freundlich isotherm equation (Equation (2)) and its derived model parameters (Table 5), the amount of CO₂ adsorbed at equilibrium (q_e) for each pressure can be computed, thus giving information on the relationship between D_e and q_e. Figure 15 delineates the effect of CO₂ adsorbed

amount at equilibrium (q_e) on the effective pore diffusivity (D_e). The variation of D_e with respect to the changes in q_e can be approximately divided into three consecutive regions for all carbons, that is, for $q_e < 40$ mg/g (Region I), $40 < q_e < 80$ mg/g (Region II) and $q_e > 80$ mg/g (Region III). For the original activated carbon (AC2), the effective diffusivity decreased sharply in Region I followed by a continuous decrease at a much slower rate over the Regions II and III. Obviously, this behavior is caused by the increasing thickness of the adsorbed layer of CO_2 that retards the diffusion of CO_2 inside the adsorbent pores. For activated carbons with different impregnation loadings of NaOH, the variation of D_e is somewhat different from that of the original carbon. The diffusivity decreased abruptly as the amount of CO_2 adsorbed increased over Region I, followed by Region II of relatively constant D_e , and again, a continuous decrease of the diffusivity in Region III. It is noted from Figure 15 that the effective diffusivity of CO_2 in activated carbons impregnated with NaOH varied in the range from 1.1×10^{-9} to 5.5×10^{-9} m^2/s and these numbers can be compared with the molecular diffusivity (D_{12}) of CO_2 in air of 1.38×10^{-5} m^2/s , estimated from the Chapman–Enskog equation for the gaseous state at low density [45]. Obviously, the resistance to mass transfer for pore diffusion of CO_2 in activated carbons is about four orders of magnitude higher than that for molecular diffusion of CO_2 outside the adsorbent particles.

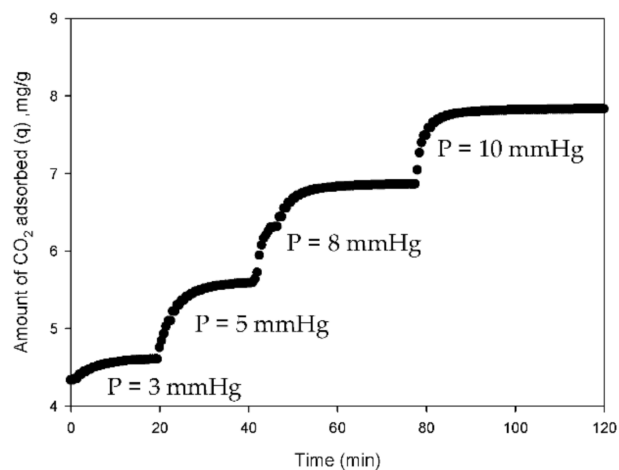


Figure 13. Typical adsorption kinetic data collected at various pressures.

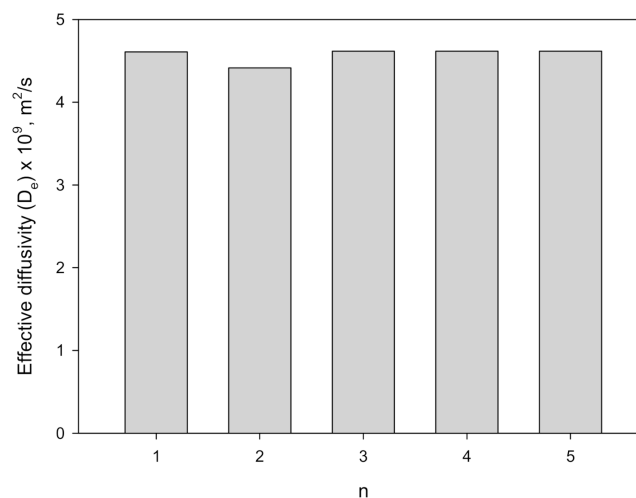


Figure 14. Typical effect of number of terms (n) in the summation solution of Equation (5) on the calculated effective diffusivity (D_e) of AC2-5 carbon sample.

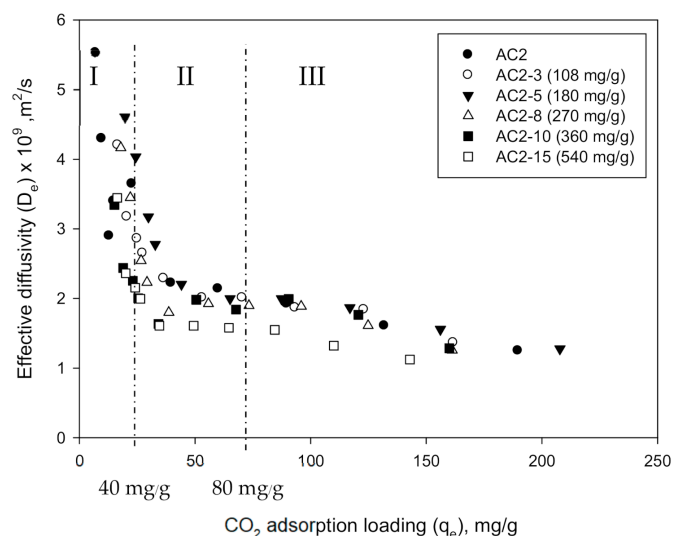


Figure 15. Effect of CO₂ adsorption loading (q_e) on the effective pore diffusivity of CO₂ (D_e) for AC2 activated carbon impregnated with varying NaOH loading.

Next, the pore sizes that accommodate the CO₂ adsorption of 40 and 80 mg/g were determined. This is achieved by first converting each amount of CO₂ adsorbed to the corresponding volume of liquid CO₂ that fills up the pores by dividing the amount adsorbed with the density of liquid CO₂ at 273 K (0.927 g/cm³). This is to assume that CO₂ exists in the adsorbed phase as a liquid-like adsorbate. The estimated volumes were found to be 0.0431 and 0.0863 cm³/g for the amount of CO₂ adsorption of 40 and 80 mg/g, respectively. Next, the pore sizes corresponding to these pore volumes can be obtained from the data of cumulative pore volume less than size calculated from the pore volume of each pore size range in Figure 12. Typical pore sizes for AC2-5 corresponding to the cumulative pore volume of 0.0431 and 0.0863 cm³/g were determined and were found to have the values of 1.41 nm and 2.8 nm, respectively. Therefore, referring to Figure 15, the transition of D_e from Region I to Region II and from Region II to Region III occurred at the approximate pore sizes of 1.41 and 2.8 nm, respectively.

The drastic decrease of D_e in Region I occurs because the pore is relatively narrow being smaller than 1.41 nm as compared to the molecular diameter of 0.334 nm for CO₂. For this reason, a slight increase in the amount of CO₂ adsorbed will drastically increase the resistance for the diffusion of CO₂ through the pores, thus giving a large decrease of the effective pore diffusivity. This effect is intensified with the alkali impregnated carbons since there is a general tendency for D_e to decrease with the increase of NaOH loading in this region. For Region II, with pore sizes in the range from 1.41 to 2.8 nm, the diffusivity is almost unaffected by the increase of CO₂ adsorption because the pore size is sufficiently large to accommodate a constant diffusion rate of CO₂ through the pores to the adsorption sites without a significant effect of mass transfer resistance, even with the presence of NaOH molecules. However, for the adsorption of CO₂ in Region III of pore sizes larger than 2.8 nm, the effective pore diffusivity was lower than that of Region II and decreased with the increase of CO₂ adsorption. This appears to indicate that the diffusive flux of CO₂ in Region III is smaller than that of Region II. It is likely that most of NaOH molecules (collision diameter of 0.38 nm) may concentrate in the smaller pores of Region I and II. The presence of NaOH in these pores could increase the concentration driving force for CO₂ transport in the pore space due to the removal of CO₂ molecules from the bulk gas by the strong affinity between CO₂ and the NaOH active sites. This will lead to the consequent increase of diffusion rate of CO₂, hence giving higher value of the effective diffusivity in Region II as compared to Region III. Obviously, the decrease of D_e in Region III should result from the increasing mass transfer resistance caused by the reduction of average pore size (pore restriction effect) when the amount of CO₂ adsorbed increased. It is also

noted from Figure 15 that for the alkali impregnated carbons, the maximum diffusivity (D_e) occurred at the optimum NaOH loading of 180 g/g coinciding with the maximum amount of CO_2 adsorbed at the same optimum loading, as shown in Figure 11.

An empirical correlation was proposed to correlate D_e with the amount of CO_2 adsorbed (q_e) and the amount of NaOH impregnation (q_a) for Regions II and III using the second-order polynomial equation for adsorption pressures up to about 100 kPa. The final derived equation, for AC2 activated carbon impregnated with sodium hydroxide and adsorption temperature of 273 K, is shown as follows.

$$D_e = (C_1 + C_2 q_a + C_3 q_a^2) + (C_4 + C_5 q_a + C_6 q_a^2) q_e + (C_7 + C_8 q_a + C_9 q_a^2) q_e^2 \quad (11)$$

where q_e = amount of CO_2 adsorbed at equilibrium = 40–200 mg/g, q_a = amount of impregnated NaOH = 108–540 mg/g. The values of the best fitted constants are, $C_1 = 2.28 \times 10^{-9}$, $C_2 = -1.90 \times 10^{-12}$, $C_3 = 1.15 \times 10^{-15}$, $C_4 = 6.00 \times 10^{-12}$, $C_5 = 9.97 \times 10^{-15}$, $C_6 = -3.00 \times 10^{-17}$, $C_7 = -6.30 \times 10^{-14}$, $C_8 = -3.00 \times 10^{-17}$, and $C_9 = 1.10 \times 10^{-19}$.

The regression coefficient of curve fitting (R^2), the maximum error, and the overall average error of prediction are 0.8721, 15.01%, and 6.09%, respectively. The comparison between the measured and the computed values of D_e is shown in Figure 16 and the general agreement is reasonably satisfactory.

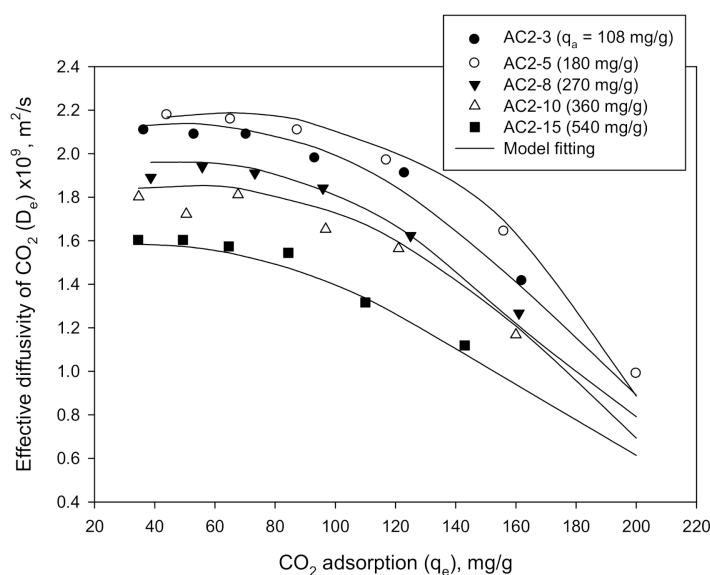


Figure 16. Comparison of experimental and computed effective pore diffusivity (D_e) in Region II and III as a function of CO_2 adsorption capacity for AC2 carbon impregnated with various loadings of NaOH.

In summary, the presence of NaOH inside the pores of activated carbon can affect the adsorption affinity of CO_2 (adsorption capacity) and the mass transport behavior of CO_2 (adsorption kinetics), the extent of which is determined by the amount of NaOH impregnation and pore structure of the original activated carbon. Furthermore, information on the equilibrium and kinetics of CO_2 adsorption at 273 K by the two types of coconut-shell activated carbons impregnated with NaOH can be readily obtained via Equations (2), (9), and (10) and Equations (6) and (11), respectively. These adsorption data are of importance for the successful design of an adsorption unit used for CO_2 adsorption with alkali impregnated activated carbons, particularly for a fixed-bed unit which is one of the most widely used adsorption systems in industry.

5. Conclusions

The following conclusion can be drawn from the study of equilibrium and kinetics of CO₂ adsorption at 273 K and a maximum pressure of 100 kPa (1 bar) by the original and NaOH impregnated activated carbon prepared from coconut shell.

All of the tested activated carbons contained mostly micropores in the range of 76 to 97% of total pore volume. The increasing of NaOH impregnation from 0 to 540 mg/g decreased continuously the specific surface area, total pore volume, and the average pore size. The reduction in these porous properties was proved to result from the decrease in the pore space due to the increasing amount of the alkali impregnant inside the pores.

Over the pressure of 100 kPa (relative pressure of 0.03), the adsorption of CO₂ at 273 K showed an initial part of Type I isotherm with the adsorption taking place by pore-filling mechanism. The amount of CO₂ adsorbed at equilibrium increased with the increasing amount of NaOH impregnation and passed through a maximum at an optimum NaOH loading of 180 mg/g, and most of adsorption occurred in the pore size range of 0.7–0.9 nm. The appearance of maximum CO₂ adsorption was hypothesized to result from the competition between the mass transfer resistance of CO₂ and the affinity of CO₂ towards NaOH adsorption sites. The CO₂ isotherm data were tested with three adsorption models and were best described by the three-parameter Sips model, followed by the Freundlich and Langmuir models. It was also noted that the adsorption of carbon dioxide in coconut shell activated carbon (with and without the impregnation of sodium hydroxide) displayed the type of physical adsorption since the amount of CO₂ adsorbed tended to decrease with the increase of temperature.

The pore diffusion model characterized by the effective pore diffusivity (D_e) was used for the analysis of CO₂ adsorption kinetics of NaOH impregnated activated carbons. Three regions for the variation of D_e versus the amount of CO₂ adsorbed could be identified which were characterized by the relative importance of pore size and the amount of impregnated NaOH. An empirical equation was proposed to correlate the effective pore diffusivity of CO₂ with the amounts of CO₂ adsorbed and the NaOH loading.

Author Contributions: C.T. contributed to the preparation of the manuscript and the supervision of experimental works; S.N. conducted the experiments; A.W., P.P. and P.B. performed the GCMC simulation and interpretation of the results. All authors have read and agreed to the published version of the manuscript.

Funding: This research was funded by Suranaree University of Technology, grant number IRD7-706-61-12-04.

Institutional Review Board Statement: Not applicable.

Informed Consent Statement: Not applicable.

Data Availability Statement: The data presented in this study will be available upon request.

Acknowledgments: We are most grateful to the financial support of this work by The SUT Research and Development Fund, Suranaree University of Technology.

Conflicts of Interest: The authors declare no conflict of interest.

References

1. IPCC Fifth Assessment Report: Climate Change 2014 (AR5), from IPCC Website. Available online: www.ipcc.ch/report/ar5/syr (accessed on 1 December 2020).
2. Khandaker, T.; Hossain, M.S.; Dhar, P.K.; Rahman, M.S.; Hossain, M.A.; Ahmed, M.B. Efficacies of carbon-base adsorbents for carbon dioxide capture. *Processes* **2020**, *8*, 654. [[CrossRef](#)]
3. Overview of Greenhouses Gas Emissions in 2018, from EPA Website. Available online: <https://www.epa.gov/ghgemissions/overview-greenhouse-gases> (accessed on 1 December 2020).
4. Carbon Dioxide, Latest Measurement (July 2020), from Website NASA Global Climate Change, Vital Signs of the Planet. Available online: <https://climate.nasa.gov> (accessed on 1 December 2020).

5. Crippa, M.; Guizzardi, D.; Muntean, M.; Schaaf, E.; Solazzo, E.; Monforti-Ferrario, F.; Olivier, J.G.J.; Vignati, E. *Fossil CO₂ Emissions of All World Countries-2020 report*, EUR 30358 EN; Publications Office of the European Union: Luxembourg, 2020; ISBN 978-92-76-21515-8.
6. Leung, D.Y.C.; Juang, R.S. Surface modifications of carbonaceous materials for carbon dioxide adsorption: A review. *Renew. Sust. Energy Rev.* **2014**, *39*, 426–443. [[CrossRef](#)]
7. Chiang, Y.C.; Juang, R.S. Surface modifications of carbonaceous materials for carbon dioxide adsorption. *J. Taiwan Inst. Chem. Eng.* **2017**, *71*, 214–234. [[CrossRef](#)]
8. Yang, H.; Xu, Z.; Fan, M.; Gupta, R.; Slimane, R.; Bland, A.E.; Wright, I. Progress in carbon dioxide separation and capture: A Review. *J. Environ. Sci.* **2008**, *20*, 14–27. [[CrossRef](#)]
9. Rashidi, N.A.; Yusup, S. An overview of activated carbons utilization for the post-combustion carbon dioxide capture. *J. CO₂ Util.* **2016**, *13*, 1–16. [[CrossRef](#)]
10. Mukherjee, A.; Okolie, J.A.; Abdelrasoul, A.; Niu, C.; Dalai, A.K. Review of post-combustion carbon dioxide capture technologies using activated carbon. *J. Environ. Sci.* **2019**, *83*, 46–63. [[CrossRef](#)]
11. Bansal, R.C.; Goyal, M. *Activated Carbon Adsorption*; CRC Press: Boca Raton, FL, USA, 2005.
12. Marsh, H.; Rodriguez-Reinoso, F. *Activated Carbon*; Elsevier: Amsterdam, The Netherlands, 2006.
13. Songolzadeh, M.; Ravanchi, M.T.; Soleimani, M. Carbon dioxide capture and storage: A general review on adsorbents. *World Acad. Sci. Eng. Technol.* **2012**, *6*, 900–907.
14. Shafeeyan, M.S.; Wan Daud, W.M.A.; Houshmand, A.; Shamiri, A. A review on surface modification of activated carbon for carbon dioxide adsorption. *J. Anal. Appl. Pyrolysis.* **2010**, *89*, 143–151. [[CrossRef](#)]
15. Boujibar, O.; Souikny, A.; Ghamouss, F.; Achak, O.; Dahbi, M. CO₂ capture using N-containing nanoporous activated carbon obtained from argan fruit shells. *J. Environ. Chem. Eng.* **2018**, *6*, 1995–2002. [[CrossRef](#)]
16. Naksusuk, S.; Tangsatitkulchai, C. Carbon dioxide capture in a fixed bed of coconut shell activated carbon impregnated with sodium hydroxide: Effects of carbon pore texture and alkali loading. *Eng. J.* **2019**, *23*, 30–48. [[CrossRef](#)]
17. Kongnoo, A.; Intharapat, P.; Worathanakul, P.; Phalakornkule, C. Diethanolamine impregnated palm shell activated carbon for CO₂ adsorption at elevated temperatures. *J. Environ. Chem. Eng.* **2016**, *4*, 73–81. [[CrossRef](#)]
18. Guo, Y.; Zhao, C.; Li, C.; Wu, Y. CO₂ sorption and reaction kinetic performance of K₂CO₃/AC in low temperature and CO₂ concentration. *Chem. Eng. J.* **2015**, *260*, 596–604. [[CrossRef](#)]
19. Tan, Y.L.; Islam, M.A.; Asif, M.; Hameed, B.H. Adsorption of carbon dioxide by sodium hydroxide-modified granular coconut shell activated carbon in a fixed bed. *Energy* **2014**, *77*, 926–931. [[CrossRef](#)]
20. Zhao, C.; Guo, Y.; Li, C.; Lu, S. Removal of low concentration CO₂ at ambient temperature using several potassium-based sorbents. *Appl. Energy* **2014**, *124*, 241–247. [[CrossRef](#)]
21. Lee, C.S.; Ong, Y.L.; Aroua, M.K.; Daud, W.M.A.W. Impregnation of palm shell-based activated carbon with sterically hindered amines for CO₂ adsorption. *Chem Eng. J.* **2013**, *219*, 558–564. [[CrossRef](#)]
22. Langmuir, I. The adsorption of gases on plane surfaces of glass, mica and platinum. *J. Am. Chem. Soc.* **1918**, *40*, 1361–1403. [[CrossRef](#)]
23. Freundlich, H. Colloid and Capillary Chemistry. *J. Chem. Educ.* **1926**, *3*, 110–134.
24. Sips, R. On the structure of a catalyst surface. *J. Chem. Phys.* **1948**, *16*, 490–495. [[CrossRef](#)]
25. Ruthven, D.M. *Principles of Adsorption and Adsorption Processes*; John Wiley & Sons: New York, NY, USA, 1984.
26. Do, D.D.; Do, H.D. Refined method of potential enhancement in the equilibria characterization of activated carbon. Comparison with GCMC and DFT. *Langmuir* **2003**, *19*, 8302–8315.
27. Harris, J.G.; Yung, K.H. Carbon dioxide's liquid-vapor coexistence curve and critical properties as predicted by a simple molecular model. *J. Phys. Chem.* **1995**, *99*, 12021–12024. [[CrossRef](#)]
28. Santoro, G.J.; Kohl, F.J.; Stearns, C.A.; Gökoglu, S.A.; Rosner, D.E. Experimental and Theoretical Deposition Rates from Salt-Seeded Combustion Gases of a Mach 0.3 Burner Rig. *NASA Tech. Pap.* **1984**, *84*, 19741.
29. Wongkoblap, A.; Junpirom, J.; Do, D.D. Adsorption of Lennard-Jones fluids in carbon slit pores of a finite length. A computer simulation study. *Adsorp. Sci. Technol. J.* **2005**, *23*, 1–18. [[CrossRef](#)]
30. Miyahara, M.; Yoshioka, T.; Nakamura, J.; Okazari, M. Simple evaluation scheme of adsorbate-solid interaction for nano-pore characterization studied with Monte Carlo simulation. *J. Chem. Eng. Japan.* **2000**, *33*, 103–112. [[CrossRef](#)]
31. Frenkel, D.; Smit, B. *Understanding Molecular Simulation*; Academic Press: New York, NY, USA, 2002.
32. Johnson, J.K.; Zollweg, J.A.; Gubbins, K.E. The Lennard-Jones equation of state revisited, *Mol. Phys. J.* **1993**, *78*, 591–618.
33. Madani, S.H.; Diaz, L.H.; Biggs, M.J.; Pendleton, P. Uncertainty in pore size distribution derived from adsorption isotherms: II. Adsorption integral approach. *Microporous Mesoporous Mater.* **2015**, *214*, 217–223. [[CrossRef](#)]
34. Cornette, V.; Villaroel-Rocha, J.; Sapag, K.; Mons, R.D.; Toso, J.P.; Lopez, R.H. Insensitivity in the pore size distribution of ultramicroporous carbon materials by CO₂ adsorption. *Carbon* **2020**, *168*, 508–514. [[CrossRef](#)]
35. Potoff, J.J.; Siepmann, J.I. Vapor-liquid equilibria of mixtures containing alkanes, carbon dioxide, and nitrogen. *AIChE J.* **2001**, *47*, 1676–1682. [[CrossRef](#)]
36. Steele, W.A. The physical interaction of gases with crystalline solids: I. Gas-solid energies and properties of isolated adsorbed atoms. *Surf. Sci.* **1973**, *36*, 317–352. [[CrossRef](#)]
37. Herrera, L.F.; Fan, C.; Nguyen, V.; Do, D.D.; Horikawa, T.; Nicholson, D. A self-consistent method to determine accessible volume, area and pore size distribution (APSD) of BPL, Norit and AX-21 activated carbon. *Carbon* **2012**, *50*, 500–509. [[CrossRef](#)]

38. Sing, K.S.W.; Everett, D.H.; Haul, R.A.W.; Moscou, L.; Pierotto, R.A.; Rouquerol, J.; Siemieniewska, T. Reporting physisorption data for gas/solid systems, with special reference to the determination of surface area and porosity, International Union of Pure and Applied Chemistry. *Pure Appl. Chem.* **1985**, *57*, 603–619. [[CrossRef](#)]
39. Rouquerol, F.; Rouquerol, J.; Sing, K. *Adsorption by Powders and Porous Solids: Principles, Methodology and Applications*; Academic Press: New York, NY, USA, 1999.
40. Gregg, S.J.; Sing, K.S.W. *Adsorption, Surface area and Porosity*; Academic Press: New York, NY, USA, 1982.
41. Do, D.D. *Adsorption Analysis: Equilibria and Kinetics*; Imperial College Press: London, UK, 1998.
42. De Souza, K.C.; Wickramaratne, N.P.; Ello, A.S.; Costa, M.J.F.; da Costa, C.E.F.; Jaroniec, M. Enhancement of CO₂ adsorption on phenolic resin-based mesoporous carbons by KOH activation. *Carbon* **2013**, *65*, 334–340. [[CrossRef](#)]
43. Wickramaratne, N.P.; Jaroniec, M. Importance of small micropores in CO₂ capture by phenolic resin-based activated carbon spheres. *J. Mater. Chem. A* **2013**, *1*, 112–116. [[CrossRef](#)]
44. Chen, L.; Watanabe, T.; Kanoh, H.; Hata, K.; Ohba, T. Cooperative CO₂ adsorption promotes high CO₂ adsorption density over wide optimal nanopore range. *Ads. Sci. Technol.* **2018**, *36*, 625–639. [[CrossRef](#)]
45. Bird, R.B.; Stewart, W.E.; Lightfoot, E.N. *Transport Phenomena*, 2nd ed.; John Wiley & Sons: Hoboken, NJ, USA, 2002.